1D fluid model of plasma profiles in the LHD divertor leg

Gakushi KAWAMURA, Yukihiro TOMITA, Masahiro KOBAYASHI and David TSKHAKAYA[1,2)]

National Institute for Fusion Science, Gifu 509-5292, Japan

[1)]*Association Euratom-ÖAW, Institute of Theoretical Physics, University of Innsbruck, Technikerstrasse 25/II, Innsbruck A-6020, Austria*

[2)]*Permanent address: Institute of Physics, Georgian Academy of Sciences, 380077 Tbilisi, Georgia*

(Received: 1 September 2008 / Accepted: 4 December 2008)

One dimensional plasma model of the divertor leg in Large Helical Device is presented. The plasma is described by stationary fluid equations for electron and ion with particle source by ionization and momentum sink by charge exchange with neutrals. Also a simple model of neutral atoms and radiative cooling by impurities are included. This model is intended to be employed in an integrated simulation where an equilibrium of the upstream plasma and plasma-surface interactions at the divertor plate are solved in different numerical codes separately. From the computational point of view, the numerical code solving the fluid equations for the divertor leg is developed for 1D flux tube where the boundary conditions of both ends are specified. The calculation time is much less than 0.1 seconds and sufficiently fast to use in future integrated simulations. Solutions for typical plasma parameters are shown in the paper. In the results, a density peaking near the wall was observed for the plasma of high density. The peaking is caused by the ion heat conduction and the collisional presheath and its sharpness increases for higher density. Also solutions for different impurity density profiles were obtained and reduction of the electron energy flux and temperature were observed. However, their effects were small and qualitative changes were not observed.

Keywords: LHD, divertor, modeling, neutral, impurity

1. Introduction

The Large Helical Device (LHD) [1] is a heliotron / tersatron type device with helical divertors [2]. Outside the core plasma, or the last closed flux surface, an ergodic layer [3] exists. It is characterized by stochastic magnetic field lines and there are no clear flux surfaces except small islands. Outside the ergodic layer, a plasma is carried along magnetic field lines toward a divertor plate. This intermediate region is called divertor leg and plays essential roles in impurity transport. The plasma profiles such as electrostatic potential and temperature determine the motion of impurities and their charge states. Therefore, physical understandings of the divertor leg and its modeling are important issues in the LHD boundary plasmas.

In this paper, we present a divertor leg model to determine the plasma profiles from input parameters such as energy flux coming from the ergodic layer and the hydrogen recycling coefficient. The model presented here is intended to be employed in our future studies as a plasma model to connect the following two simulation codes; EMC3 code [3] for the ergodic layer and ERO code [4] for divertor surface. The former solves fluid equations to obtain equilibrium plasma profiles in the ergodic magnetic field and the latter solves the equations of motion for impurity particles to obtain the sputtering yield, time evolution of surface conditions and impurity transport near a target plate. In order to avoid a numerical difficulty arising from the strong magnetic shear in the LHD divertor plasma and to keep the amount of the computational resources in reasonable level, we employ simple 1D model along the magnetic field line, or flux tube model, in the paper. Since hundreds of flux tubes will be necessary and also iterations technique will be employed to obtain self-consistent solutions, the calculation time of each flux tube has to be sufficiently short, e.g. much less than one second.

The detail of the formulation is presented in Sec. 2.1. Fundamental equations are fluid equations with ionization source, charge exchange momentum loss and impurity cooling. They are similar to those in other modelings and simulation studies [5–8] except the boundary conditions and the model of neutral atoms, which are introduced in Sec. 2.2 and Sec. 2.3, respectively. In Sec. 3, numerical solutions of our model are shown and their physical interpretations and effects of impurities are discussed. Finally in Sec. 4, conclusions are presented.

2. Divertor leg model

2.1 Fluid equations

We compare time scales of the divertor plasma. Particle dwell time in the divertor leg is estimated as $\tau_{\rm dwell} \sim l_{\rm c}/(c_{\rm s}/2)$. Here $c_{\rm s}$ and $l_{\rm c}$ represent the ion sound speed and the connection length of the divertor leg, i.e. length along a magnetic field line, respectively. For a typical set of plasma parameters, temperature $T \sim 40$eV, magnetic field $B \sim 2$T, density $n \sim 10^{19}$m^{-3} and connection length $l_{\rm c} \sim 3$m, the dwell time is given by $\tau_{\rm dwell} \sim 2$ms for a hydrogen plasma. Temperature equilibration time, $\tau_{\rm eq}$, defined by $(d/dt)\ln|T_{\rm i} - T_{\rm e}| = \tau_{\rm eq}^{-1}$ is estimated as $\tau_{\rm eq} \sim 0.5$ms. Temperature anisotropy times, $\tau_{\rm a}^{\rm e}$ and $\tau_{\rm a}^{\rm i}$, defined by $(d/dt)\ln|T_\perp - T_\parallel| = \tau_{\rm a}^{-1}$ are estimated as $\tau_{\rm a}^{\rm e}/\tau_{\rm a}^{\rm i} = \sqrt{m_{\rm e}/m_{\rm i}} \sim 0.02$ and $\tau_{\rm a}^{\rm i} \sim 0.03$ms. The above four

author's e-mail: kawamura.gakushi@nifs.ac.jp

time scales satisfy the relation $\tau_{\rm dwell} > \tau_{\rm eq} \gg \tau_{\rm a}^{\rm i} \gg \tau_{\rm a}^{\rm e}$. We can, therefore, assume $T_\perp = T_\parallel$ for both electrons and ions, while both the ion and electron temperatures should be solved individually.

The following assumptions and notations are employed in this work. The divertor plasma profiles are assumed to be 1D along the magnetic field line. The spatial coordinate variable is denoted by s and the origin of the coordinate, $s = 0$, is chosen at the boundary between the ergodic layer and the divertor leg. The other end, $s = l_{\rm c}$, is located at the boundary between the collisional presheath and the magnetic presheath [9], which is a very thin layer in front of the divertor plate. The boundary condition at the magnetic presheath entrance is given by equality of the Bohm criterion, i.e. the flow velocity v along the magnetic field becomes the ion sound speed $c_{\rm s}$. The flow velocity is assumed to be ambipolar, $v_{\rm e} = v_{\rm i} = v$, and the quasineutral condition is satisfied, $n_{\rm e} = n_{\rm i} = n$. The plasma includes neutral hydrogen atoms and the collisions between the plasma and the neutrals cause electron impact ionizations and charge exchanges. Their rate coefficients are denoted by $\langle\sigma_{\rm iz}v\rangle$ and $\langle\sigma_{\rm cx}v\rangle$ respectively, and calculated by Lotz model [10] and Freeman-Jones model [11]. The plasma temperature is assumed to be relatively high so that the recombination is negligible. Density of the neutrals is denoted by $n_{\rm n}$. Its determination is discussed in Sec. 2.2 and thus we regard $n_{\rm n}$ as a given function of the position in this section.

1D stationary fluid equations describing the divertor plasma are given by the following five equations. i) and ii) Density and momentum conservations:

$$\frac{dm_{\rm i}nv}{ds} = \langle\sigma_{\rm iz}v\rangle\, m_{\rm i}n_{\rm n}n, \tag{1}$$

$$\frac{d}{ds}\left[m_{\rm i}nv^2 + n\,(T_{\rm e}+T_{\rm i})\right] = -\langle\sigma_{\rm cx}v\rangle\, m_{\rm i}n_{\rm n}nv, \tag{2}$$

where the electron and ion masses and temperatures were denoted by $m_{\rm e}$, $m_{\rm i}$, $T_{\rm e}$ and $T_{\rm i}$. The right-hand sides represent plasma source due to ionization and momentum sink due to charge exchange. iii) and iv) Energy conservations for electrons and ions:

$$\begin{aligned}\frac{d}{ds}&\left[\frac{5}{2}nvT_{\rm e} - \kappa_{\rm e0}T_{\rm e}^{5/2}\frac{dT_{\rm e}}{ds}\right]\\ &= env\frac{d\phi}{ds} - \frac{3m_{\rm e}n}{m_{\rm i}}\nu_{\rm eq}(T_{\rm e}-T_{\rm i})\\ &\quad -25e\,\langle\sigma_{\rm iz}v\rangle\, n_{\rm n}n - Lnn_{\rm imp},\end{aligned} \tag{3}$$

$$\begin{aligned}\frac{d}{ds}&\left[\frac{m_{\rm i}nv^3}{2} + \frac{5}{2}nvT_{\rm i} - \kappa_{\rm i0}T_{\rm i}^{5/2}\frac{dT_{\rm i}}{ds}\right]\\ &= -env\frac{d\phi}{ds} + \frac{3m_{\rm e}n}{m_{\rm i}}\nu_{\rm eq}(T_{\rm e}-T_{\rm i})\\ &\quad -\langle\sigma_{\rm cx}v\rangle\, n_{\rm n}n\left(\frac{3}{2}T_{\rm i} + \frac{1}{2}m_{\rm i}v^2\right),\end{aligned} \tag{4}$$

where the potential was denoted by ϕ. The heat conduction coefficients and temperature equilibration coefficient are given by $\kappa_{\rm i0} = 1.2\times10^{69}{\rm W/mJ^{7/2}}$, $\kappa_{\rm e0} = 5.0\times10^{67}{\rm W/mJ^{7/2}}$ and $\nu_{\rm eq} = 6.9\times10^{17}nT_{\rm e}^{3/2}$ [12]. The density of impurities and the radiative cooling rate coefficient were denoted by $n_{\rm imp}$ and $L(T_{\rm e})$. For simplicity, the impurity density is assumed to be proportional to the plasma density, i.e. $n_{\rm imp}/n = r_{\rm imp} = {\rm const}$. In addition to the energy transfer due to the electric field and the temperature equilibration, the radiation loss during the ionization and the kinetic energy loss caused by the charge exchange are introduced to the electron and ion energy equations, respectively. v) Ohm's law, or electron momentum conservation:

$$e\frac{d\phi}{ds} = \frac{1}{n}\frac{dnT_{\rm e}}{ds} + 0.71\frac{dT_{\rm e}}{ds}. \tag{5}$$

The second term of the right-hand side represents thermal force.

In order to simplify Eqs. (1) – (5) to a set of first order differential equations, we introduce the following variables; flux $G \equiv nv$, momentum flux $P \equiv m_{\rm i}nv^2 + n\,(T_{\rm e}+T_{\rm i})$, electron and ion energy fluxes $Q_{\rm e} \equiv 5nvT_{\rm e}/2 - \kappa_{\rm e0}T_{\rm e}^{5/2}dT_{\rm e}/ds$ and $Q_{\rm i} \equiv m_{\rm i}nv^3/2 + 5nvT_{\rm i}/2 - \kappa_{\rm i0}T_{\rm i}^{5/2}dT_{\rm i}/ds$. The fluid equations are rewritten with these new set of variables as follows:

$$\frac{dG}{ds} = \langle\sigma_{\rm iz}v\rangle\, n_{\rm n}n, \tag{6}$$

$$\frac{dP}{ds} = -m_{\rm i}\,\langle\sigma_{\rm cx}v\rangle\, n_{\rm n}nv, \tag{7}$$

$$\begin{aligned}\frac{dQ_{\rm e}}{ds} &= env\frac{d\phi}{ds} - \frac{3m_{\rm e}n}{m_{\rm i}}\nu_{\rm eq}(T_{\rm e}-T_{\rm i})\\ &\quad -25e\,\langle\sigma_{\rm iz}v\rangle\, n_{\rm n}n - Lr_{\rm imp}n^2,\end{aligned} \tag{8}$$

$$\begin{aligned}\frac{dQ_{\rm i}}{ds} &= -env\frac{d\phi}{ds} + \frac{3m_{\rm e}n}{m_{\rm i}}\nu_{\rm eq}(T_{\rm e}-T_{\rm i})\\ &\quad -\langle\sigma_{\rm cx}v\rangle\, n_{\rm n}n\left(\frac{3}{2}T_{\rm i} + \frac{1}{2}m_{\rm i}v^2\right),\end{aligned} \tag{9}$$

$$\frac{dT_{\rm e}}{ds} = \frac{1}{\kappa_{\rm e0}T_{\rm e}^{5/2}}\left(\frac{5}{2}nvT_{\rm e} - Q_{\rm e}\right), \tag{10}$$

$$\frac{dT_{\rm i}}{ds} = \frac{1}{\kappa_{\rm i0}T_{\rm i}^{5/2}}\left(\frac{1}{2}mnv^3 + \frac{5}{2}nvT_{\rm i} - Q_{\rm i}\right), \tag{11}$$

$$\begin{aligned}e\frac{d\phi}{ds} &= 1.71\frac{dT_{\rm e}}{ds} - \frac{T_{\rm e}}{P-2m_{\rm i}uG}\\ &\quad\times\left(2m_{\rm i}u\frac{dG}{ds} - \frac{dP}{ds} + n\frac{dT_{\rm e}}{ds} + n\frac{dT_{\rm i}}{ds}\right).\end{aligned} \tag{12}$$

We note that the density and velocity are employed in the right-hand sides of the new set of equations for convenience; $n = \left(P + \sqrt{P^2 - 4m_{\rm i}(T_{\rm e}+T_{\rm i})G^2}\right) \Big/ 2(T_{\rm e}+T_{\rm i})$ and $v = G/n$. The condition for the density to be a real number is given by $u \le \sqrt{(T_{\rm e}+T_{\rm i})/m_{\rm i}} \equiv c_{\rm s}$. It implies that the ion is isothermal.

2.2 Neutral model

In order to know the dominant dynamics over the neutral gas near the divertor plate, we estimate the mean-free-path (MFP) of the hydrogen atoms (H-H collision). The neutral density observed near the divertor plate in the LHD is usually 10^{18} to $10^{19}{\rm m^{-3}}$. From the hydrogen's Bohr

radius $r_B = 5.3 \times 10^{-11}$m and a typical neutral density $n_n = 10^{19}$m^{-3}, the cross section and the MFP are calculated as $\sigma = 4\pi r_B^2 = 3.5 \times 10^{-20}$m^{-2} and $\lambda_n = 1/\sqrt{2} n_n \sigma = 2.0$m, respectively. Since the length of the divertor leg is roughly one meter, the neutral gas is almost collisionless.

Therefore, a hydrogen atom released from the surface keeps its velocity until it experiences an ionization or a charge exchange. For simplicity, the flow velocity of the neutrals is treated as a constant in this work although the charge exchange processes can change the velocity of the neutrals through the collision. The decrease in the number of the neutrals is given by the ionizations and thus, the neutral density n_n is determined by the equation of the flux conservation:

$$\frac{dv_n n_n}{ds} = -\langle \sigma_{iz} \rangle n_n n, \tag{13}$$

where the flow velocity of neutrals was denoted by v_n. Ions hitting the wall surface are neutralized and hydrogen molecules are released with the thermal velocity of the wall temperature. The molecules are much slower than the atoms and ions and thus, they are localized near the surface. In this work, we assume that the molecules are dissociated immediately by electron impacts and the hydrogen atoms with Frank-Condon energy are created. The average flow velocity of atoms is estimated from the Frank-Condon energy; $v_n \simeq -\sqrt{3e/\pi m_i} \simeq 1 \times 10^4$ m/s.

2.3 Boundary conditions

Eqs. (6) – (13) describes the equilibrium profiles of the divertor plasma and the neutrals. These differential equations can be solved by integrating them from one end to the other numerically. In this work, we integrated them from the wall side because the most of the boundary conditions are determined physically at $s = l_c$.

In the remainder of this paper, we use variables with subscripts '0' and '1' to express the boundary values at $s = 0$ and l_c, respectively. We employed four boundary conditions and four fixed plasma parameters to solve the eight differential equations. i) Flow velocity v becomes the ion sound speed c_s at $s = l_c$.

$$v_1 = c_s \equiv \sqrt{\frac{T_e + T_i}{m_i}}. \tag{14}$$

This condition corresponds to the Bohm criterion along the magnetic field at the magnetic presheath entrance. ii) and iii) Electron and ion energy fluxes at $s = l_c$ are determined by the sheath theory [12, 13].

$$Q_{e1} = \frac{1}{2} n_1 v_1 T_{e1} \left[4 + \ln \frac{m_i}{2\pi m_e} - \ln\left(1 + \frac{T_i}{T_e}\right) \right], \tag{15}$$

$$Q_{i1} = \frac{1}{2} n_1 v_1 \left(T_{e1} + 6 T_{i1} \right). \tag{16}$$

iv) Flux of the neutrals at $s = l_c$ is determined by the recycling coefficient R.

$$v_n n_{n1} = -R n_1 v_1, \quad v_n = -\sqrt{\frac{3e}{\pi m_i}}. \tag{17}$$

v) Plasma density at $s = 0$ is fixed to a given value n_0. vi) and vii) Electron and ion energy fluxes at $s = 0$ is fixed to a given value $Q_{e0} = Q_{i0} = Q_0/2$. viii) Potential at $s = l_c$ is fixed to $\phi_1 = 0$. Since this model is intended to be employed for the connection of the two codes, i.e. EMC3 and ERO, at the both ends, $s = 0$ and l_c, we chose the boundary value at $s = 0$ for density and energy flux. The input parameters of this model are as follows; density n_0, total energy flux Q_0, connection length l_c and recycling coefficient R.

3. Results and discussions

We have developed a computational code to solve the fluid equations (6) – (13). They are integrated numerically from the wall side, $s = l_c$, by the fourth order Runge-Kutta method. The step width of the spatial integration is changed adoptively in each step of the Runge-Kutta method to keep the numerical error sufficiently low and to minimize the calculation time. The width is determined so that the change of the potential between the current and previous grid points is kept smaller than a certain value, e.g. $\Delta\phi = 0.01 T_e/e$ in this work. The deviation of the potentials solved for $\Delta\phi = 0.01 T_e/e$ and $0.005 T_e/e$ was less than 0.1% and the number of grid points for $\Delta\phi = 0.01 T_e/e$ was approximately 200. In order to find a correct solution satisfying given boundary values of n, Q_e and Q_i at $s = 0$, we employed a shooting method with iterations. By using results of previous step, more suitable boundary values at $s = l_c$ are determined by the multi-dimensional Newton's method. The total calculation time including the iterations is much less than 0.1 seconds on an ordinary PC.

We show plasma profiles for typical parameters in Fig. 1. The parameters used in the calculation are as follows; $l_c = 3$m, $R = 0.9$, $r_{imp} = 0$, $n_0 = 5 \times 10^{18}$/m^3 and $Q_0 = 10$MW/m^2. The distance between a X-point and a divertor plate is 0.5–1m in the normal direction and the connection length is 2–3m. Typical plasma density and temperature are found in Ref. [14]. Although the recycling coefficient R affects the neutral density and plasma flux, its effects are rather restrictive and does not cause qualitative changes on the plasma profiles. Therefore, we use a fixed recycling coefficient in the calculations here. The density profile of neutrals is shown in Fig. 1(a). Since the neutral density is determined by Eq. (13) and the boundary condition, Eq. (17), the maximum value, $n_{n1} \simeq 1.2 \times 10^{19}$, and the length of the collisional presheath, $L_{CP} \simeq 0.3$m, depend on the other parameters. In the simple neutral model used here, the neutral density at $s = l_c$ is determined by the average velocity v_n and the recycling flux $R n_1 v_1$. Therefore, the neutral density increases when the plasma density and temperature increase. The characteristic length of the decreasing neutral density n_n along the magnetic field, or shortly decay length, increases when plasma density decreases because less ionizations take place. The fact that the decay length is shorter than the connection length, $l_c = 3$m, im-

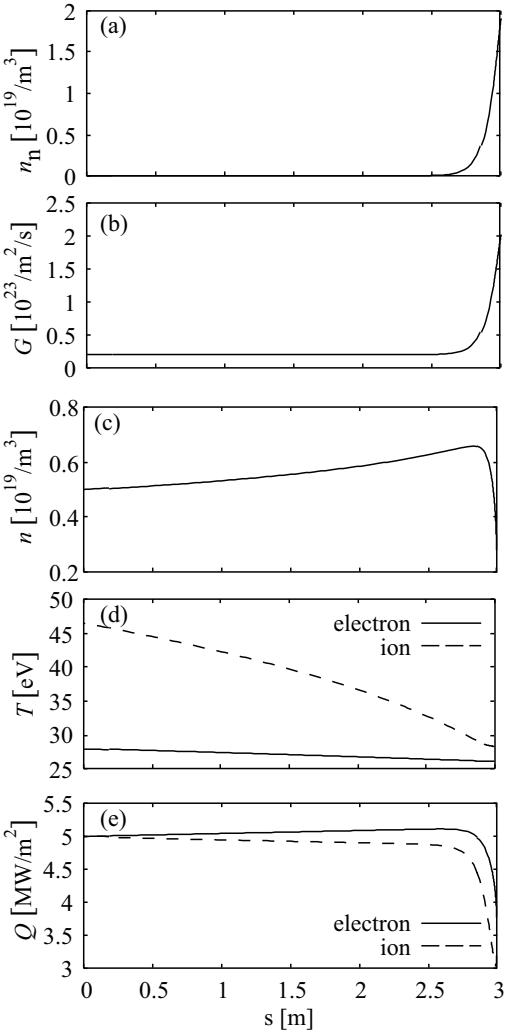

Fig. 1 Spatial profiles along a filed line of (a) neutral density n_n, (b) particle fluxes G, (c) plasma density n, (d) temperatures T_e, T_i, (e) energy fluxes Q_e, Q_i.

plies the ionization of all the neutrals released from the wall surface. As shown in Fig. 1(b), the ionization increases the particle flux near the wall. Since the recycling coefficient is less than unity here, the input flux is finite at $s = 0$.

The profile of the plasma density is plotted in Fig. 1(c). A collisional presheath is formed in front of the wall and its width is approximately 0.3m in this case. The gradual increase in the region, $s < 2.7$m, is caused by the ion temperature gradient shown in Fig. 1(d). Since the neutral density is very low compared with n_{n1}, the energy is conserved and thus the pressure $n(T_e + T_i)$ is constant. Therefore, the temperature drop, $d(T_e + T_i)/ds < 0$, yields the density rise, $dn/ds > 0$. The temperature drop sustains the energy flux by the heat conduction. The gradient of T_e is smaller than that of T_i because the heat conductively of electrons is much higher than that of ions. These mechanisms cause the density peaking near the wall and its sharpness increases for the plasma of higher density.

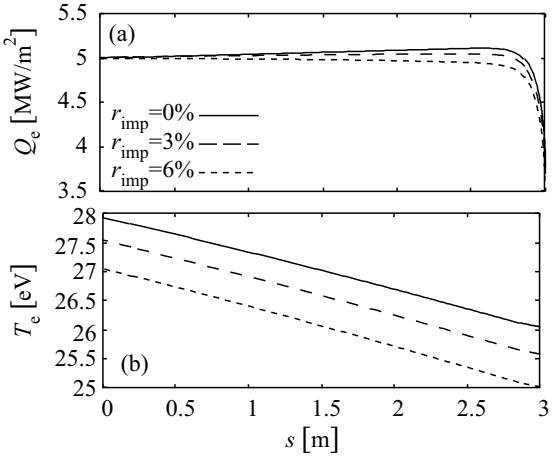

Fig. 2 Electron energy flux (a) and temperature (b) for three different ratios of carbon impurity, r_{imp} = 0, 3 and 6%.

The energy fluxes shown in Fig. 1(e) are almost constant in the region, $s < 2.5$m, because the heat transfer from ions to electrons are much less than the energy fluxes. The drop near the wall is formed by the collisions with neutrals. The charge exchange and ionization cause the ion and electron energy losses, respectively.

Secondly we analyzed the effects of carbon impurities on the divertor plasma. In the fluid model used here, the radiation loss is included in the electron energy flux equation. The profiles of the electron energy fluxes for three different ratios of carbon impurity, r_{imp} = 0, 3 and 6%, in Fig. 2(a). Large impurity ratio yields rapid decrease of the electron energy flux. The total energy flux $Q_0 = Q_{e0} + Q_{i0}$ is reduced by 0.2MW/m^2 when r_{imp} is increased from 0% to 6%. The electron temperature shown in Fig. 2(b) is also affected by impurities. The temperature gradient does not change but the value becomes small for large impurity ratio because of the boundary condition of Q_e at $s = l_c$, Eq. (15). The electron energy flux Q_{e1} reduced by the radiative cooling yields low temperature at $s = l_c$. Although we omitted figures of other plasma parameters, we confirmed that they have little or no dependences on the impurity ratio.

4. Conclusions

A fluid model of LHD divertor leg plasma along the magnetic field line was presented. The model is intended to be employed in the future simulation studies with EMC3 and ERO codes. In order to keep the computational cost low, 1D simple fluid equations and an equation of continuity for neutral atoms were adopted. The calculation code was developed to solve these equations with boundary conditions relevant to code connections at the both end of the calculation region. The plasma profiles are calculated by integrating the equations from the wall side. The boundary conditions are specified at both ends, $s = 0$ and l_c, and solutions satisfying them are obtained by iterations with the multi-dimensional Newton's method. The calculation time

is much less than 0.1 seconds and it is sufficiently short for the code integration.

Plasma profiles for various sets of plasma parameters were obtained by solving the fluid equations. Characteristics of neutral density, flux, plasma density, temperature and energy flux were discussed. Dependences of the neutral density profile on other parameters and their physical interpretations were elucidated. For example, a density peaking near the wall is caused by the ion heat conduction and the collisional presheath. Its sharpness increases for higher density plasma. Effects of the radiative cooling by carbon impurities on plasma profiles were also analyzed and small reduction of the electron energy flux and temperature are observed. Other parameters such as density and ion temperature are not affected by the impurity. We conclude that our simple model yields physically reasonable solutions of the divertor plasma at low computational cost.

In the paper, we employed simple neutral and impurity models as a preliminary. Atomic processes of hydrogen molecules and atoms such as dissociation and ionization which reflect on their reaction rates and characteristic energies are essential elements and the implementation to the code is in progress. The fluid treatment of impurities is also important to obtain the impurity profiles and realistic radiative cooling. These improvements and the application of the model to the integrated simulation will be presented in future publications.

Acknowledgments

The contribution of the last author was carried out under the European Fusion Development agreement, supported by the European Communities. The views and opinions expressed herein do not necessarily reflect those of the European Commission. This work was supported in part by a Grant-in-Aid for scientific research from Ministry of Education, Science and Culture of Japan (No. 19055005).

[1] N. Oyabu *et al.*, Nucl. Fusion, **34**, 387 (1994)
[2] N. Oyabu *et al.*, J. Nucl. Mater., **266–269**, 302 (1999)
[3] M. Kobayashi *et al.*, J. Nucl. Mater., **363–365**, 294 (2007)
[4] A. Kirschner *et al.*, Nuclear Fusion, **40**, 989 (2000)
[5] P. C. Stangeby and J. D. Elder, J. Nucl. Mater., **196-198**, 258 (1992)
[6] K. Shimizu *et al.*, J. Nucl. Mater., **196-198** 476 (1992)
[7] Rajiv Goswami *et al.*, Phys. Plasmas, **8**, 857 (2001)
[8] Deok-Kyu Kim and Sanh Hee Hong, Phys. Plasmas, **12**, 062504 (2005)
[9] D. Tskhakaya and S. Kuhn, Plasma Phys. Control. Fusion, **47**, A327 (2005)
[10] W. Lotz, Astrophys. J. Suppl., **14**, 207 (1967).
[11] R. L. Freeman and E. M. Jones, *Atomic Collision Processes in Plasma Physics Experiments*, Culham Laboratory, Abingdon, England, Report CLM-R 137 (1974).
[12] Peter C. Stangeby, *The Plasma Boundary of Magnetic Fusion Devices*, Institute of Physics Publishing (Bristol and Philadelphia 1999).
[13] G. D. Hobbs and J. A. Wesson, Plasma Phys., **9**, 85 (1967).
[14] S. Masuzaki *et al.*, Nucl. Fusion, **42**, 750 (2002)